THE COMPOSITION OF X-RAY AMORPHOUS MATERIALS IN GALE CRATER, MARS. S. L. Simpson[1], C. N. Achilles[2], E. B. Rampe[1], T. F. Bristow[3], D. F. Blake[3], S. J. Chipera[4], D. T. Vaniman[4], R. T. Downs[5], D. W. Ming[1], R. V. Morris[1], S. M. Morrison[6], V. M. Tu[7], M. T. Thorpe[8], A. S. Yen[9], D. J. Des Marais[2], G. Downs[10], J. P. Grotzinger[11], R. M. Hazen[6], A. H. Treiman[12], N. Castle[3], P. I. Craig[3], R. Gellert[13], E. M. Hausrath[14], T. S. Peretyazhko[7], L. M. Thompson[15], B. Tutolo[16], J. A. Berger[7], [1]NASA Johnson Space Center, Houston, TX, USA (sarah.l.simpson@nasa.gov), [2]NASA GSFC, [3]NASA Ames, [4]PSI, [5]Univ. Arizona, [6]Carnegie Institution for Science, [7]Jacobs at NASA JSC, [8]UMD/GSFC, [9]JPL, [10]Stanford Univ., [11]Caltech, [12]LPI, [13]UG, [14]UNLV, [15]UNB, [16]Univ. Calgary.

Introduction: One of the most surprising discoveries by the CheMin X-ray diffractometer instrument in Gale Crater is the omnipresent X-ray amorphous material observed in each of the 36 drill samples and three sediment samples collected to date [1-3]. The term 'amorphous' generally describes any phase that lacks long-range atomic order; here we use the term 'X-ray amorphous materials' to include nanocrystalline phases that scatter X-rays (i.e., they may contain short-range atomic order below the resolution of the X-ray diffractometer). This X-ray amorphous component is a major constituent (~20-70 wt %) of rock and soil samples in Gale Crater, indicated by a characteristic hump in the X-ray diffraction patterns between ~25 and 30° 2θ [1-4]. The origin of these materials on Mars remains speculative, but terrestrial analogue studies help shed light on how these may have formed [5-8]. Naturally occurring amorphous materials are found in a variety of environments; on Earth, these can be primary (e.g., volcanic or impact-produced glass) or secondary (e.g., aqueous alteration of a primary phase) products. In Gale Crater, the X-ray amorphous component could be primary glass(es) deposited via aeolian or fluvial processes, secondary aqueous alteration products or chemical precipitates [1-5, 9-12]; it is likely to be a combination of all of these, and determining the origin of this material is a challenging endeavor.

Recently, Curiosity left the Fe/Mg phyllosilicate-rich Glen Torridon region, traversed the clay-sulfate transition and arrived at the sulfate unit at drill hole "Canaima" (CA) (Fig. 1) [13]. The transition from the phyllosilicate-bearing strata to the sulfate unit was marked by mineralogical trends initially observed by pre-mission remote sensing datasets; the most distinct of these trends was the transition from older Fe/Mg smectite-rich sandstones and mudstones in Glen Torridon to the younger phyllosilicate-barren, hydrated Mg-sulfate-bearing sandstones [13,14]. These stark mineralogical and geochemical trends can be traced across the planet and are thought to represent a change from a warm and wet to cold and dry climate [15,16]. Despite the dramatic paleoenvironmental changes preserved in the geology of Gale Crater, the X-ray amorphous material has persisted in each and every drilled sample. In this contribution, we present the major compositional trends of the X-ray amorphous component through the clay-sulfate transition and sulfate unit, and place these new data within the context of the regional geology. We also provide a traverse-wide overview of the variation in amorphous material composition and discuss potential paleoenvironmental indicators.

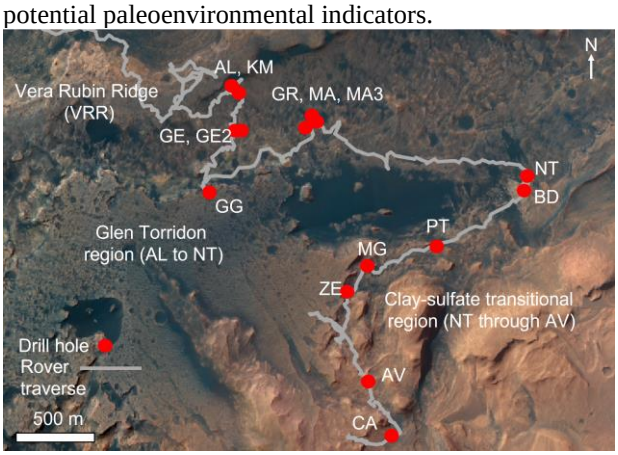

Figure 1: Curiosity's traverse and drill hole locations from the Fe/Mg-smectite-bearing Glen Torridon region (drill locations AL to NT) and the Clay-Sulfate transitional region (drill locations NT through AV); the final drill hole shown here, Canaima (CA), marks the first drill hole into the sulfate unit.

Methods: The composition of the bulk amorphous material is determined using a mass balance calculation, wherein the bulk mineralogy and crystal chemistry, as determined by CheMin XRD Rietveld refinements, is subtracted from the bulk sample geochemical data as determined by the Alpha-Particle X-ray Spectrometer (APXS) [2, 4, 9, 17]. APXS post-sieve dump pile analyses were used when available, to be most consistent with the CheMin analyses; when these were not available, analyses on the drill bit tailings were used. Phyllosilicate abundances and types were estimated using a combination of FULLPAT [18] and Sample Analysis at Mars (SAM) datasets. The abundance of amorphous material was also determined using FULLPAT. For several samples, the amount of amorphous material was underestimated by FULLPAT which yielded unrealistic (negative) oxide abundances. In these scenarios, the amount of amorphous material in a sample was increased until a realistic (non-negative) composition was reached. This method is not without uncertainties and assumptions (e.g., ideal crystal chemistry for some minerals) but it provides a

rough estimate to examine overall trends in the amorphous material composition, which when combined with other instrument datasets can help shed light on the regional trends and origin of the amorphous material across all drilled units in Gale Crater.

Results and Discussion: *Trends in amorphous material composition*: The amorphous material is primarily comprised of the major oxides SiO_2, FeO_T, MgO, CaO and SO_3; other oxides are present but often form less than ~3 wt % of the sample. This composition suggests the amorphous component is dominated by secondary materials and so, together with the sample mineralogy it can be used to constrain past aqueous conditions. When considering the amorphous and crystalline fractions together, generally, high SiO_2 indicates an open, acidic system, or possibly hydrothermal conditions; a composition dominated by FeO_T suggests a more oxidizing environment; and an amorphous composition with elevated SO_3 suggests an environment conducive to salt precipitation, or at least conditions cold and stable enough to prevent crystallization and preserve the sulfate as an amorphous phase. The sample Windjana contained the lowest abundance of amorphous material at ~18 wt%, and the highest amount of amorphous material has been detected in Lubango at ~64 wt% (determined by FULLPAT). Based on a combination of FULLPAT and minimum amorphous value calculations (see methods), the amorphous component SiO_2 remained relatively low in the Bradbury group (~18 to 33 wt%) compared to other sections; there was an increase in SiO_2 in the Murray formation (~34 to 76 wt%), with the sample Buckskin reaching the highest observed SiO_2 content across the entire mission at ~76 wt%. In general, amorphous material associated with alteration haloes contain higher SiO_2. The amorphous material in sample Windjana, in the Bradbury group, contains the highest FeO_T.

Trends across the clay-sulfate transition: Through the clay-sulfate transition the amount of amorphous material in each sample ranges from ~41 to ~54 wt% (based on FULLPAT values); if we consider both FULLPAT and the minimum amorphous component calculated values, the amount of amorphous material appears to increase slightly through the traverse with Zechstein (ZE) containing the highest amorphous abundance (~75 wt%). When we compare these datasets, normalized to 100 wt%, the most obvious trend in amorphous material composition is the increase in SiO_2 which appears to be anti-correlated with SO_3 abundance; a similar pattern can be observed in some samples throughout the entire traverse, prior to reaching the clay-sulfate transition and sulfate unit. In this section there is no apparent pattern in FeO content, however preliminary calculations suggest there is a noticeable increase in MgO that correlates with the increase in SO_3 in the most recent drill sample, Canaima (using the FULLPAT amorphous abundance, ~15 wt%, MgO and ~24% wt% SO_3) [19,20]. There appears to be a slight increase in Al_2O_3 through the transitional unit which decreases along with SiO_2 in Canaima. The composition of the amorphous material calculated in Canaima is consistent with a magnesium sulfate-rich phase.

The clay sulfate transition and sulfate unit is marked by the disappearance of phyllosilicates; a 10Å phyllosilicate, interpreted as a collapsed smectite [10], is abundant at the base of the section in drill samples Nontron (NT) and Bardou (BD) (17.8 and 12.2 wt % phyllosilicates as determined by FULLPAT, respectively), with Pontours containing only trace amounts (2.8 wt %); above these strata the phyllosilicates disappear completely, the amorphous component becomes enriched in SiO_2 before decreasing sharply in the sulfate unit (Canaima, CA), which contains the first and only detection of crystalline polyhydrated Mg-sulfate (to date) [13,14]. It is possible that this increase in amorphous SiO_2 in the upper portion of the clay-sulfate transition may be a result of phyllosilicate dissolution or from a phyllosilicate precursor that never crystallized.

The mineralogical and sedimentological trends observed in this region indicate a period of rapid drying and sulfate-rich groundwaters [10]; the composition of the amorphous component also changes in this area, although the fate (or complete absence) of phyllosilicates in this area, and their relationship to the composition of the amorphous material is still up for debate.

References: [1] Rampe, E., et al. (2020) *Geochemistry, 80 (125605)*. [2] Achilles, C. et al., (2020) *JGR Planets, 125(8)* [3] Bristow, T. et al., (2021) *Science Advances, 4, eaar3330.* [4] Thorpe, M. at el., (2022) *JGR Planets 127* [5] Rampe, E. et al., (2022) *EPSL 584, 117471*. [6] Thorpe, M. et al., (2022) *53rd LPSC, #1200.* [7] Simpson, S. et al., (2022*) 53rd LPSC, #1549.* [8] Simpson, S. et al., (2023) *this conference.* [9] Smith, R., et al. (2021) *JGR Planets 126.* [10] Schieber, J. et al., (2022) *Sed., 69*, 2371-2435. [11] Meslin, P.-Y., et al., (2013) *Science, 341,* 6153. [12] David, G. et al., (2022) *GRL, 49*(21). [13] Rampe, E. et al., (2023) *this conference*. [14] Chipera S. J. et al. (2023, *submitted*) *Science* [15] Sheppard, Y. et al. (2020) *JGR, 126*(2). [16] Bibring J.-P. et al. (2006) *Science, 312,* 400-404. [17] Gellert, R. et al., (2015), *Ele., 11*(1), 39-44. [18] Chipera, S. et al., (2002) *J. App. Cry*. 35, 744-749. [19] Berger, J. et al., (2023) *this conference*. [20] Thompson, L. M. et al., (2023) *this conference*. SLS is funded through a NASA Postdoctoral Program appointment at NASA Johnson Space Center.